Applied Catalysis B: Environmental 328 (2023) 122535

Contents lists available at ScienceDirect

Applied Catalysis B: Environmental

journal homepage: www.elsevier.com/locate/apcatb

Highly selective synthesis of light aromatics from CO_2 by chromium-doped ZrO_2 aerogels in tandem with HZSM-5@SiO_2 catalyst

Lijun Zhang, Weizhe Gao *, Fan Wang, Chengwei Wang, Jiaming Liang, Xiaoyu Guo, Yingluo He, Guohui Yang, Noritatsu Tsubaki *

Department of Applied Chemistry, School of Engineering, University of Toyama, Gofuku 3190, Toyama 930-8555, Japan

ARTICLE INFO

Keywords:
Tandem catalyst
Aerogels
HZSM-5@SiO_2
CO_2 hydrogenation
Light aromatics

ABSTRACT

The efficient utilization of CO_2 has great strategic significance, especially for the reduction of the CO_2 concentration in the atmosphere and relief of the dependence on the fossil resources. Although direct conversion of CO_2 to aromatics via a methanol-mediated pathway has made great progress recently, how to selectively synthesize light aromatics (benzene, toluene and xylenes) remains a great challenge for the perspective of industrial demand. In this work, a highly active tandem catalyst composed of chromium-doped ZrO_2 aerogel and HZSM-5@SiO_2 zeolite was employed for the hydrogenation of CO_2 to light aromatics. The ZrO_2-Cr/HZSM-5@SiO_2 catalyst achieved 13.9% CO_2 conversion, 76.8% aromatics selectivity and 51.2% light aromatics selectivity. It was worth noting that the CO selectivity was suppressed to about 29%, while the CH_4 selectivity was controlled at around 1%. The external Brønsted acid sites of HZSM-5 zeolite were eliminated by silylation. This modification could inhibit the alkylation of light aromatics and enhance the light aromatics selectivity. The novel ZrO_2-Cr/HZSM-5@SiO_2 catalyst opens a new avenue for the oriented transformation of CO_2 molecules into valuable light aromatics and provides a new insight for the directed design of tandem catalysts.

1. Introduction

The rapid development of economy promotes the increasing demand of energy in society, which makes the urgent replacement for the traditional energy structures [1,2]. The unlimited use of traditional carbon resources (such as oil, coal and natural gas) has caused a sharp increase for the concentration of carbon dioxide (CO_2) in the atmosphere. This leads to a series of environmental problems such as global warming, ocean acidification and so on [3,4]. CO_2 is a substance with abundant carbon sources. In nature, green plants can convert CO_2 and store chemical energy through photosynthesis. If CO_2 is recycled and selectively converted into high-energy-density fuels or chemicals by artificial means, it not only changes the traditional energy structures but also greatly relieves environmental problems [5]. Research on CO_2 hydrogenation to produce hydrocarbons has been benefiting from a modified iron-based Fischer-Tropsch (FT) synthesis [6–8]. Firstly, the CO_2 was converted to CO via reverse water-gas shift (RWGS) reaction over the iron catalyst and CO was hydrogenated to linear hydrocarbons simultaneously [8]. It is well known that the products of FT synthesis follow the Anderson-Schulz-Flory distribution and the distribution of linear hydrocarbons is not concentrated [8,9]. In order to obtain target product with high selectivity, it is possible to directly tailor complex hydrocarbons to target product, but this process is full of challenging [9–11].

Aromatics (especially light aromatics: benzene, toluene and xylenes) are important bulk chemicals, which are widely used in the production of solvents, pharmaceuticals, dyes, fuel additives, and various polymers [8,12–14]. Currently, aromatics are mainly derived from petroleum refining, which is an environmentally unfriendly process with high energy consumption [14–16]. To solve this problem, the researchers developed a new route for direct synthesis of aromatics by CO_2 hydrogenation [8,14]. Generally, the synthesis of aromatics mainly includes a modified FT synthesis or a methanol-mediated pathways [17,18]. The modified FT synthesis is based on the light olefins, and subsequently zeolite is employed to produce aromatics through light olefins oligomerization, cyclization and dehydroaromatization [19]. Gao et al. designed a Na-FeMn/HZSM-5@Silicalite-1 catalyst for direct conversion of CO_2 to aromatics [20]. The para-xylene (PX) selectivity could be enhanced by the tandem catalyst of Na-FeMn and capsule-like HZSM-5@Silicalite-1 [20]. Wei et al. passivated the external Brønsted

* Corresponding authors.
E-mail addresses: gaowzh@eng.u-toyama.ac.jp (W. Gao), tsubaki@eng.u-toyama.ac.jp (N. Tsubaki).

https://doi.org/10.1016/j.apcatb.2023.122535
Received 4 January 2023; Received in revised form 19 February 2023; Accepted 23 February 2023
Available online 24 February 2023

acid sites of HZSM-5 zeolite by silylation process and explored the effect of HZSM-5 zeolite with different Brønsted acid sites for the synthesis of light aromatics and coke formation during CO_2 hydrogenation, achieving 32.3% light aromatics selectivity [21]. In the methanol-mediated route, oxide/zeolite is used as a tandem catalyst, in which oxide catalyst converts CO_2 to methanol, and zeolite is responsible for transforming methanol to aromatics. Some tandem catalysts for the synthesis of aromatics have been developed successively, including Cr_2O_3/HZSM-5 [2], $ZnZrO_x$/HZSM-5 [8,12,14,22], $ZnAlO_x$/HZSM-5 [23], $ZnCrO_x$/HZSM-5 [14,24] and so on. In the above two routes, zeolite is an important part of the tandem catalyst for CO_2 hydrogenation to aromatics. Until now, some significant progresses have been achieved in the selective synthesis of aromatics, PX and tetramethylbenzene from CO_2 or CO hydrogenation [25]. However, the oriented synthesis of light aromatics from CO_2 hydrogenation remains a great challenge.

In this work, a new ZrO_2-Cr/HZSM-5@SiO_2 tandem catalyst was developed for direct conversion of CO_2 to light aromatics with high selectivity by one step. The CH_4 selectivity was controlled at around 1% when the CO_2 single-pass conversion reached 13.9%, and the selectivity of light aromatics was as high as 51.2% in all hydrocarbons. A highly active chromium-doped ZrO_2 aerogel catalyst was successfully obtained by sol-gel synthesis combined with CO_2 supercritical drying. HZSM-5@SiO_2 zeolite was produced by silylation of HZSM-5, which passivated the external Brønsted acid sites of HZSM-5 zeolite, effectively inhibiting the alkylation reaction of light aromatics. The oxygen vacancies on the surface of ZrO_2-Cr aerogel were the sites for CO_2 adsorption and activation. The methanol intermediates firstly formed on the ZrO_2-Cr surface and subsequently directly converted to light aromatics over HZSM-5@SiO_2. The construction of novel ZrO_2-Cr aerogel and HZSM-5@SiO_2 zeolite tandem catalyst provides a new avenue for the development of CO_2 conversion. In particular, it opens a feasible new scheme for the controllable and highly selective synthesis of light aromatics.

2. Experimental section

2.1. Preparation of aerogel catalysts

A typical synthesis method of sc-ZrO_2-Cr aerogel catalyst was as follows, firstly, 0.016 mol $ZrO(NO_3)_2$•2 H_2O and 0.002 mol $Cr(NO_3)_3$•9 H_2O were dissolved in 100 mL 75% ethanol solution. After the above solution was stirred at room temperature for 1 h, 1.3 g formamide and 20.1 g 1,2-propylene oxide were added into the mixture. After 1 h stirring at room temperature, the precursor was heated in a 70 °C water bath until gelation. The wet gel was solvent-exchanged with ethanol and sealed into an autoclave. Supercritical CO_2 flowed into the autoclave through a high-pressure pump to keep the pressure in the autoclave at about 7.5 MPa. The autoclave was then heated up to 260 °C and held for 60 min for CO_2 supercritical drying. The dried solid was calcined at 550 °C for 5 h, and the resulting catalyst was denoted as sc-ZrO_2-Cr (8:1). ZrO_2-Cr catalysts with different Cr-doping contents were synthesized by the above method. By adjusting the content of $Cr(NO_3)_2$•9 H_2O, sc-ZrO_2-Cr aerogels with different Zr/Cr molar ratios (16:1, 4:1 and 1:1) could be obtained. Without supercritical drying, sd-ZrO_2-Cr was prepared by the same method as above with a Zr/Cr ratio of 8:1.

co-ZrO_2-Cr was prepared by the co-precipitation method. Typically, solution A was prepared by dissolving 0.08 mol $ZrO(NO_3)_2$•2 H_2O and 0.01 mol $Cr(NO_3)_3$•9 H_2O in 90 mL distilled water and heating it to 70 °C. Subsequently, 0.2 mol $(NH_4)_2CO_3$ was dissolved in 200 mL water to obtain solution B. The A and B solutions were added dropwise to a beaker at the same time, and then precipitated at 70 °C, as the pH was controlled at 7–8 under stirring. After aging at room temperature, the above mixture was washed with distilled water and collected by filtration. The product was dried at 120 °C overnight and calcined at 550 °C for 5 h. The resulting samples are labeled as co-ZrO_2-Cr.

hy-ZrO_2-Cr was prepared by hydrothermal method. Firstly, 0.04 mol $ZrO(NO_3)_2$•2 H_2O and 0.005 mol $Cr(NO_3)_3$•9 H_2O were dissolved in 45 mL distilled water. Then 20 mL 1 M $(NH_4)_2CO_3$ solution was gradually added dropwise to the solution. The mixture was subsequently transferred to the reactor for the hydrothermal reaction at 180 °C for 10 h. After centrifugation, washing and drying, the target catalyst could be collected and named as hy-ZrO_2-Cr.

2.2. Preparation of zeolite catalysts

HZSM-5 zeolite samples with different Si/Al ratios were prepared by hydrothermal method. Briefly, tetraethoxysilane (TEOS), $Al(NO_3)_3$•9 H_2O, 25% tetrapropylammonium hydroxide (TPAOH), and ethanol (EtOH) were dissolved in distilled water at a molar ratio of SiO_2: Al_2O_3: H_2O: TPAOH: EtOH = 1:1/(2X):50:0.24:4, where X is the atomic ratio of Si/Al. After magnetic stirring for 4 h, the resulting clear solution was transferred to a Teflon-sealed autoclave and kept in a 180 °C oven for 24 h. After being cooled down to room temperature, the obtained solid product was washed with distilled water, dried at 120 °C overnight, and calcined at 550 °C in the air for 5 h.

The HZSM-5@SiO_2 core-shell zeolite samples were prepared by the chemical liquid deposition (CLD) method. Firstly, 1 g HZSM-5 was immersed in *n*-hexane of 7 g. Subsequently, 1.7 g TEOS was added dropwise to the mixture. After stirring for 4 h, the temperature of the mixture was raised from room temperature to 80 °C to evaporate *n*-hexane. Finally, the HZSM-5@SiO_2 core-shell zeolite was obtained after calcination at 550 °C for 5 h. Repeating the above process could obtain composite zeolite with different SiO_2 shell thicknesses. The above SiO_2 shell coating process was conducted twice, where sample was denoted as HZSM-5@SiO_2-2.

Tandem catalysts are prepared by physical mixing. The oxide and zeolite catalysts were mixed in a 1:2 weight ratio and ground in an agate mortar for 3 min. Subsequently, 20–40 mesh particles could be obtained by being pressed, pulverized, and sieved under about 60 MPa. To study the proximity effect, single sc-ZrO_2-Cr and HZSM-5@SiO_2-2 were also sieved to 20–40 mesh. The particles of the two samples were then mixed well by shaking them in the container.

2.3. Characterization methods

2.3.1. Catalyst characterization

XRD patterns of the catalysts were collected at room temperature using a Rigaku RINT 2400 system diffractometer by employing Cu-Kα (40 kV, 40 mA) radiation. The morphology of the catalyst was observed by a JEOL JSM-6360LV scanning electron microscope (SEM) equipped with a JED-2300 energy dispersive spectrometer (EDS) accessory. The morphology of oxide catalyst was observed using a FEI Tecnai G2 F30 transmission electron microscope (TEM). Elemental composition of the zeolite and metal oxide catalyst powder were determined by a wave-dispersive X-ray fluorescence (XRF, Philips Magix-601) spectrometry. Valence state information of the catalyst was collected by a Thermo Fisher Scientific ESCALAB 250Xi X-ray photoelectron spectroscopy equipped with an in-situ reduction pretreatment chamber. The binding energy (BE) was calibrated by using C 1 s line with BE value of 284.6 eV. Nitrogen physisorption and desorption measurements were performed using a BELSORP MAX II-334 instrument to obtain specific surface area, pore volume and pore size. The samples were degassed at 200 °C for about 4 h before catalyst analysis. Ammonia temperature-programmed desorption (NH_3-TPD), Hydrogen temperature-programmed desorption (H_2-TPD) and CO/CO_2 temperature-programmed desorption (CO-TPD and CO_2-TPD) were tested on a BELCAT-B-TT catalyst analyzer equipped with a thermal conductivity detector (TCD). The pretreatment process of the sample was as follows. Firstly, 50 mg catalyst was treated in 30 mL min^{-1} He atmosphere at 300 °C for 1 h. Next, it was cooled to 50 ℃ and saturated with NH_3. The catalyst was purged with He at the same temperature to remove physisorbed NH_3. Finally, the temperature was programmed from 100 to 650 °C at a heating rate of 10 °C min^{-1} in a He

atmosphere. The experimental procedure of H_2-TPD and CO-TPD was the same as that of NH_3-TPD, but the gas was changed to the corresponding H_2 and CO gas. For CO_2-TPD, the sample was pretreated at 400 ℃ for 2 h under a flow of pure H_2 and saturated in CO_2 at 50 °C, and then the temperature was increased to 750 °C at the rate of 10 °C min^{-1}. Other experimental procedures are similar to those of NH_3-TPD. In-situ diffuse reflectance infrared Fourier transform spectroscopy (DRIFTS) was performed using a NICOLET iS50 FT-IR spectrometer. All catalysts were pretreated with H_2 at 400 °C for 2 h and then cooled to 390 °C. The background spectrum was recorded at a resolution of 2 cm^{-1}. Subsequently, when CO_2/H_2 (molar ratio = 1/3) was fed into the reactor and the reaction pressure reached 3 MPa, in situ Drift spectra were collected with a resolution of 2 cm^{-1}. The thermogravimetric curve of the spent catalyst was tested by SHIMADZU DTG-60. The temperature was programmed from room temperature to 900 °C at a heating rate of 10 °C/min in air.

2.3.2. CO_2 hydrogenation test

Before the reaction, the catalyst was pretreated at 400 °C under the atmosphere of pure H_2 (60 mL min^{-1}) for 4 h. After being cooled down to room temperature, feed gas (24.02 vol% CO_2, 4.03 vol% Ar and H_2 balance) was fed into the reactor. Typical reaction pressure and temperature are 4 MPa and 360 °C, respectively. The reaction effluent was quantitatively analyzed in full online using three gas chromatographs (GC-2014, Shimadzu). The first chromatograph was equipped with flame ionization detector (FID) and HP-PLOT/Q column for hydrocarbon analysis, the second chromatograph was equipped with FID and HP-INNOWAX column for further identify the xylene isomers and the third chromatograph was equipped with TCD and activated carbon columns for Ar, CO, CH_4, and CO_2 analysis. To suppress condensation that might occur during the reaction, the piping from the catalyst bed to the gas chromatograph was heated to 200 °C. CO_2 conversion and hydrocarbon C-mol selectivity were calculated according to the following equations:

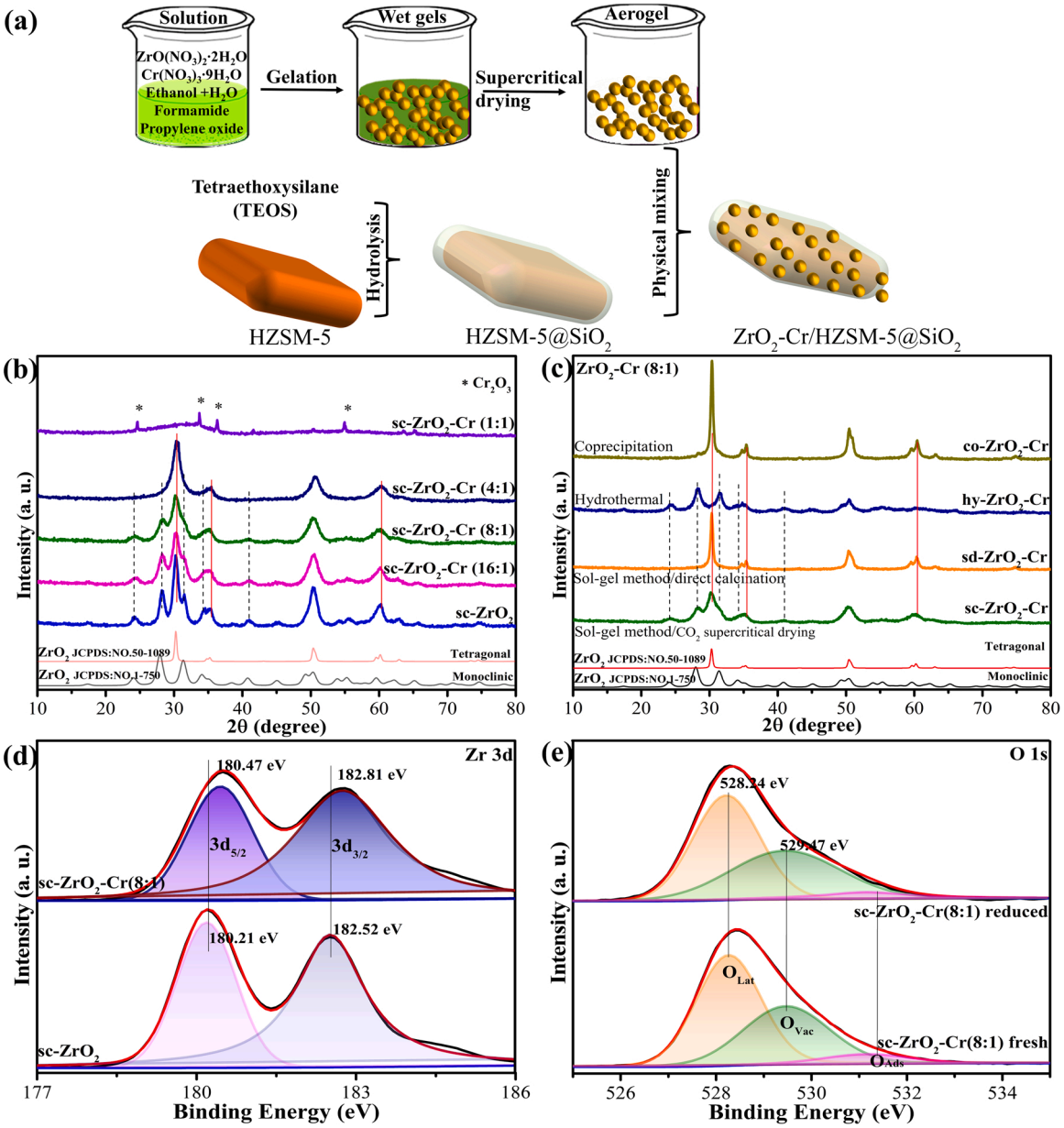

Fig. 1. (a) Schematic diagram of the catalyst synthesis of the ZrO_2-Cr/HZSM-5@SiO_2 catalyst; (b) XRD patterns of ZrO_2 and ZrO_2-Cr (n:1, n = 16, 8, 4, 1.) samples prepared by CO_2 supercritical drying; (c) XRD patterns of ZrO_2-Cr (8:1) samples prepared by different synthesis methods; (d) XPS fine spectra of Zr element in sc-ZrO_2 and sc-ZrO_2-Cr (8:1). (e) XPS fine spectra comparison of O element fresh and after reduction of sc-ZrO_2-Cr (8:1).

$$CO_2 Conversion = \frac{CO_2 inlet - CO_2 outlet}{CO_2 inlet} \times 100\%$$

Where *CO_2 inlet* and *CO_2 outlet* represent mole fractions of CO_2 at the inlet and outlet, respectively.

$$Sel_{C_nH_m} = \frac{nC_nH_m outlet}{\sum_1^n nC_nH_m outlet} \times 100\%$$

CO was formed via the reverse water gas shift and its selectivity was calculated according to:

$$COselectivity = \frac{COoutlet}{CO_2 inlet - CO_2 outlet} \times 100\%$$

Where *COoutlet* represent mole fractions of CO at the outlet. CO was not included in hydrocarbon and MeOH/DME selectivity calculation, as its selectivity calculation method was different.

3. Results and discussion

3.1. Structure and morphology of catalysts

ZrO_2-Cr aerogel catalysts with different amounts of Cr were synthesized by a sol-gel method combined with CO_2 supercritical drying method (Fig. 1(a)). A series of aerogel catalysts with different Zr/Cr molar ratios, which were denoted as sc-ZrO_2-Cr (n:1, n was the molar ratio of Zr to Cr), were obtained by adjusting the contents of introduced chromium. The XRD patterns of sc-ZrO_2 and sc-ZrO_2-Cr (n:1, n = 16, 8, 4, 1) catalysts were shown in Fig. 1(b). The pure ZrO_2 aerogel catalyst, which obtained by the sol-gel method combined with CO_2 supercritical drying, shown a kind of tetragonal and monoclinic mixed crystal phase structure, as displayed in Fig. 1(b) [12]. The diffraction peaks at 24.2°, 28.1°, 31.5°, 34.3° and 40.8° could be assigned to the (110), (−111), (111), (020) and (102) planes of the monoclinic ZrO_2 (JCPDS 1–750), respectively. While the diffraction peaks at 30.3°, 35.4°, and 60.3° were correspond to the (011), (110) and (121) planes of the tetragonal ZrO_2 (JCPDS 50–1089) [14,22].

With increasing the content of Cr from sc-ZrO_2-Cr (16:1) to sc-ZrO_2-Cr (4:1), the diffraction peaks intensity of the monoclinic phase was decreased, and ZrO_2-Cr (4:1) was almost pure tetragonal structure. After increasing the Cr content to 1:1, sc-ZrO_2-Cr (1:1) catalyst was obtained. For sc-ZrO_2-Cr (1:1) catalyst, it was obvious that the sample exhibited relative high crystallinity of Cr_2O_3. The diffraction peaks at 24.5°, 33.6°, 36.3° and 55.1° were correspond to the (012), (104), (110) and (116) crystal planes of orthorhombic Cr_2O_3 (JCPDS 3–1124). As shown in Table S1, the doping amounts of Cr in the specific catalysts were measured by XRF. The XRD patterns of different ZrO_2-Cr (Zr/Cr 8:1) catalysts prepared by different methods were compared in Fig. 1(c). The co-ZrO_2-Cr with a typical tetragonal structure was prepared by the coprecipitation method. The hydrothermally synthesized hy-ZrO_2-Cr shown a typical monoclinic structure. Without CO_2 supercritical drying, the sd-ZrO_2-Cr samples prepared by sol-gel method exhibit typically tetragonal structure.

To further understand the effect of Cr doping on the ZrO_2-Cr aerogel catalysts, X-ray photoelectron spectroscopy (XPS) technique was employed. Fig. 1(d) showed the XPS fine spectrum comparison of Zr elements before and after ZrO_2 doping with Cr. In the fine spectrum of Zr 3d, two peaks of Zr 3d3/2 and Zr 3d5/2 were found, whose corresponding binding energies were 182.52 eV and 180.21 eV, respectively [26,27]. After doped with chromium, the signal peaks of Zr 3d were shifted to higher binding energy. XPS fine spectra of Cr 2p were shown in Fig. S1(a). The binding energies of Cr 2p3/2 and Cr 2p1/2 were located at 575.53 eV and 585.21 eV, respectively, which could be assigned to Cr^{III} in Cr_2O_3 [14]. In addition, 578.05 eV and 587.31 eV may correspond to the binding energies of Cr^{VI} [28]. After H_2 reduction, the Cr 2p peak of ZrO_2-Cr (8:1) shifted to lower binding energy. In addition, the signal of Cr^{VI} basically disappeared after H_2 reduction. Three distinct O 1 s signal peaks were identified in the XPS spectrum of the ZrO_2-Cr (8:1) sample (Fig. 1(e)). The peaks at 528.24 eV and 529.47 eV correspond to lattice oxygen atoms (O_{Lat}) and oxygen vacancies near oxygen atoms (O_{Vac}), respectively [29,30]. The peak at 531.18 eV was associated with the hydroxyl oxygen (O_{Ads}) adsorbed on the catalyst surface [31]. Oxygen vacancies on the external surface of ZrO_2-Cr catalyst were favorable to C-O bond activation, which made ZrO_2-Cr become a possible catalyst for CO_2 activation and hydrogenation synthesis of methanol [2,32]. The oxygen vacancy concentration was measured by the area ratio of O_{Vac} to O_{Lat} signal peaks. After H_2 reduction, the O_{Vac}/O_{Lat} value of pure sc-ZrO_2 was 0.62 (Fig. S1(b)). For sc-ZrO_2-Cr (8:1) catalyst, after H_2 reduction, the O_{Vac}/O_{Lat} value increased from 0.67 to 0.75 (Fig. 1(e)). The introduction of Cr enhanced the surface properties of the composite catalyst, which could generate more surface vacancies and more active sites and promote CO_2 hydrogenation performance.

Advanced CO_2 supercritical drying technology could largely maintain the pores and network of ZrO_2-Cr aerogel catalysts [33,34]. The N_2 adsorption-desorption isotherms and pore size distributions of the CO_2 supercritical dried samples were shown in Fig. S2(a). The CO_2 supercritical dried ZrO_2 and ZrO_2-Cr (n:1, n = 16, 8, 4, 1.) samples exhibited typical type IV adsorption-desorption isotherms with obvious H2 hysteresis loops [35], indicating these samples have mesoporous structure. The sc-ZrO_2 aerogel catalyst had a surface area of 60 m^2g^{-1} after calcination (Table S2). After doping with Cr, the specific surface area of sc-ZrO_2-Cr (16:1) was significantly improved to 126 m^2g^{-1}. The specific surface areas of the sc-ZrO_2-Cr catalysts were increased, when the Cr doping amount was further increased. The specific surface area of sc-ZrO_2-Cr (8:1) was 163 m^2g^{-1}, which was higher than those of co-ZrO_2-Cr and hy-ZrO_2-Cr (Table S2). Without using CO_2 supercritical drying, the surface area of sd-ZrO_2-Cr (sol-gel method) was reduced to 76 m^2g^{-1}, which was not favorable to CO_2 conversion [8,24]. The N_2 adsorption-desorption isotherms of ZrO_2-Cr (8:1) samples prepared by different synthetic methods were shown in Fig. S2(b). Using the BJH method, the pore size distributions of the samples were compared in Fig. S2(c). It was obvious that the CO_2 supercritical drying technology was beneficial to the retention of pore structure. Pores existed in ZrO_2-Cr aerogel, which the pores size mainly distributed in the range of 0–20 nm. With increasing the Cr doping amount, the pore volume increased, the average pore size continued decreasing (Table S2), while the smaller pore structure enhanced the specific surface area [36,37]. The sd-ZrO_2-Cr sample was dried directly, and the generated porous during gelation collapsed simultaneously. Thus, sd-ZrO_2-Cr sample exhibited fewer pores than sc-ZrO_2-Cr sample (Fig. S2(d)). The sample prepared by the coprecipitation method (co-ZrO_2-Cr) also exhibited a small amount of microporous structure, and the specific surface area was only 39 m^2g^{-1}. The hy-ZrO_2-Cr sample synthesized by hydrothermal method displayed typical IV isolines and H3 hysteresis loop, indicating that it has mesoporous properties [36]. The pore size distribution curve in Fig. S2(d) indicates that the hy-ZrO_2-Cr sample has a stacked pore structure.

The SEM of sc-ZrO_2-Cr (8:1) aerogel nanoparticles was shown in Fig. 2(a). It was obvious that the serious aggregation of nanoparticles. Fig. 2(b) was the TEM image of sc-ZrO_2-Cr (8:1), the average particle size of sc-ZrO_2-Cr (8:1) was calculated to be 4.6 nm. The HR-TEM image of sc-ZrO_2-Cr (8:1) catalyst showed lattice spacings of 0.21 nm and 0.26 nm, corresponding to the (012) lattice planes of tetragonal ZrO_2 and the (020) lattice planes of monoclinic ZrO_2 (Fig. 2(c)). The HZSM-5 zeolite sample exhibited an elliptical shape with smooth sides (Fig. 2(d)). The HZSM-5@SiO_2-X (X represents the number of chemical liquid deposition conducts) core-shell zeolite samples were constructed by introducing amorphous SiO_2 on the external surface of HZSM-5 zeolite via CLD method. In Fig. 2(e), it could be seen that the surface of HZSM-5 was rough, and there were some fine amorphous SiO_2 on the surface. The XRD results of HZSM-5 before and after coating with SiO_2 were compared in Fig. S3. The XRD patterns of HZSM-5@SiO_2 and HZSM-5

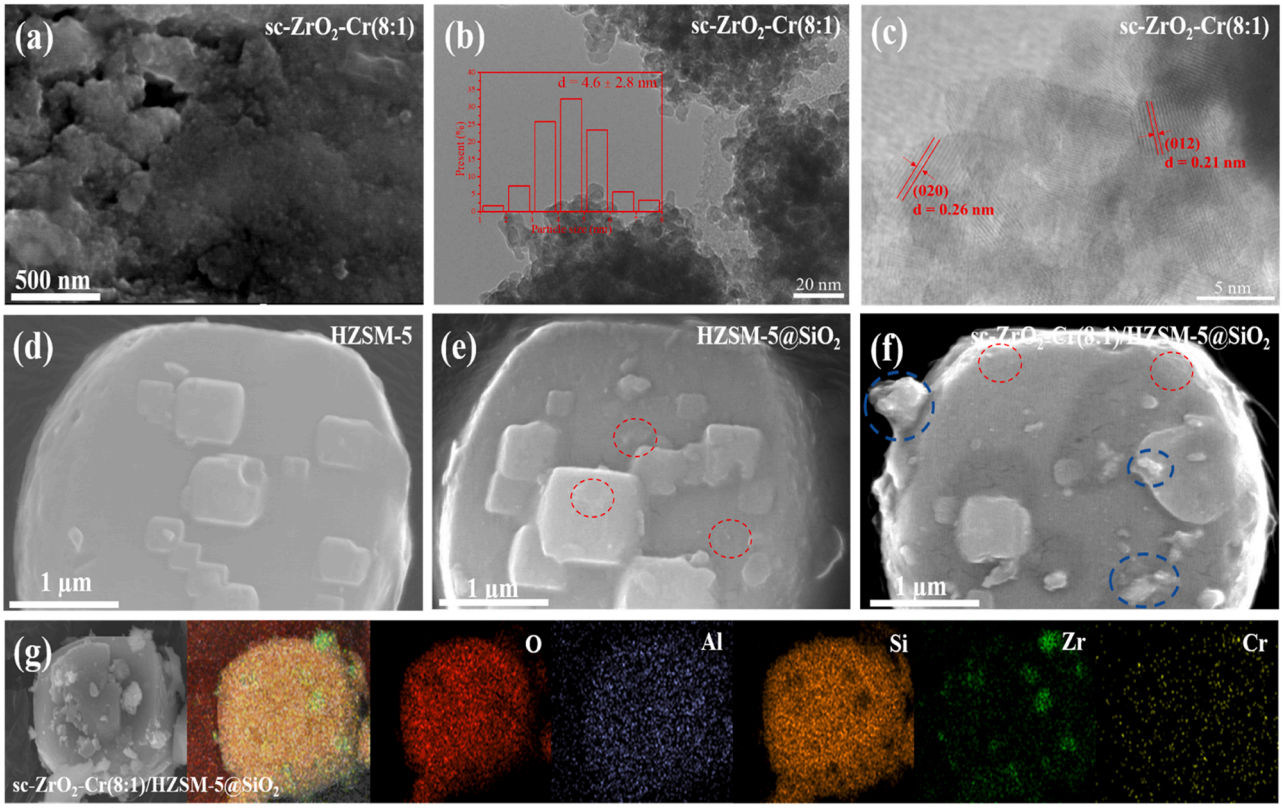

Fig. 2. sc-ZrO_2-Cr (8:1) oxide (a) SEM, (b) TEM (the inset shown particle distribution of sc-ZrO_2-Cr (8:1) catalyst) and (c) HR-TEM images. (d) HZSM-5 zeolite, (e) HZSM-5@SiO_2 core-shell zeolite and (f) sc-ZrO_2-Cr (8:1)/HZSM-5@SiO_2 tandem catalyst SEM images. (g) Elemental distribution of sc-ZrO_2-Cr (8:1)/HZSM-5@SiO_2 composite catalyst.

were the same, and no peaks belonging to amorphous SiO_2 were detected. The Al 2p XPS spectra of HZSM-5 and HZSM-5@SiO_2-2 zeolites were exhibited in Fig. S4. The original HZSM-5 zeolite displayed a significant peak at 75.0 eV, which was attributed to the presence of Al on the external surface. For HZSM-5@SiO_2 zeolite, no peak belonging to Al was detected. This result indicated that the core-shell HZSM-5@SiO_2 zeolite was constructed successfully. The SEM image of sc-ZrO_2-Cr (8:1)/HZSM-5@SiO_2 tandem catalyst prepared by powder-mixing method were shown in Fig. 2(f). The HZSM-5@SiO_2 core-shell zeolite still showed an elliptical shape with a size about 3–5 μm. sc-ZrO_2-Cr nanoparticles were dispersed on the external surface of HZSM-5@SiO_2 core-shell zeolite (Fig. S5). The interface between sc-ZrO_2-Cr and HZSM-5 was a physical interaction and the two components maintained their respective independent structures. The sufficient mixing between sc-ZrO_2-Cr and HZSM-5@SiO_2 was beneficial to reducing the agglomeration of sc-ZrO_2-Cr nanoparticles. Meanwhile, the maximum degree of contact between the two catalysts could promote synergistic effect. Fig. 2(g) exhibited the element distribution of sc-ZrO_2-Cr (8:1)/HZSM-5@SiO_2. It could be seen that sc-ZrO_2-Cr were distributed on the zeolite.

3.2. *Effects of different Si/Al ratios of zeolites and their distance with aerogel catalyst on catalytic performances*

Light aromatics (benzene, toluene and xylenes (BTX)), constituting the main market for aromatics, were the most important aromatics products due to their wide industrial applications [20,21,38]. In this work, oxide/zeolite tandem catalysts composed of chromium-doped ZrO_2 and HZSM-5 zeolites were used for CO_2 hydrogenation to BTX. The catalytic performances of CO_2 hydrogenation over different ZrO_2-Cr/HZSM-5 catalysts were shown in Fig. 3. Before reaction, all catalysts were pretreated under pure H_2 flow (60 mL min^{-1}) at 400 °C for 4 h. Fig. 3(a) displayed the results of the effect of different Si/Al ratios on CO_2 hydrogenation performances under the reaction conditions of 4 MPa, 1200 mL/g_{cat}/h and 360 °C. The tandem catalyst contained sc-ZrO_2-Cr (8:1) aerogel catalyst and HZSM-5 zeolites with different Si/Al ratios. The HZSM-5 zeolites Si/Al ratios were measured by XRF, as shown in Table S3. As the Si/Al ratio of HZSM-5 zeolite increased, the CO_2 conversion decreased from 11.2% to 7.5%. The CO selectivity increased from 39.7% to 60.9%. The HZSM-5 zeolite with Si/Al ratio of 130 achieved the highest aromatics selectivity of 75.2% with CO_2 conversion of 9.1%. It is worth noting that the formation of light olefins increased with further increasing Si/Al ratio, while aromatics selectivity decreased. These results indicated the high Si/Al zeolites exhibited insufficient aromatization ability [20,21]. As the Si/Al ratio of HZSM-5 zeolite increased from 28 to 318, the aromatics selectivity firstly increased from 37.8% to 75.2% and then decreased to 56.9%. Table S4 and Table S5 showed the products distribution obtained from sc-ZrO_2-Cr (8:1) composed HZSM-5 with different Si/Al ratios. Among all of the aromatics, the heavy aromatics (C_{9+}) was the main product.

It was worth mentioning that the HZSM-5 zeolite with 130 Si/Al ratio was a potential candidate for producing light aromatics, and the selectivity of BTX in all hydrocarbons was 21.1%. It was generally believed that Brønsted acid sites exist on the external surface and pore region of HZSM-5 zeolite [32,39]. Light aromatics formed within the micropores of HZSM-5 zeolite, and these were easily alkylated to heavier aromatics during diffusion to the external surface of HZSM-5 zeolite [40]. To obtain BTX with high selectivity, the HZSM-5 zeolite was encapsulated by SiO_2, which was specifically realized by the CLD process. The external Brønsted acid sites of HZSM-5 zeolite were passivated by silylation treatment. Compared with original HZSM-5, the crystallinity of HZSM-5@SiO_2 zeolite did not change significantly after CLD modification (Fig. S3). For HZSM-5 and HZSM-5@SiO_2-X zeolites, the ratio of Si/Al slightly increased from 130 to 139 with different number

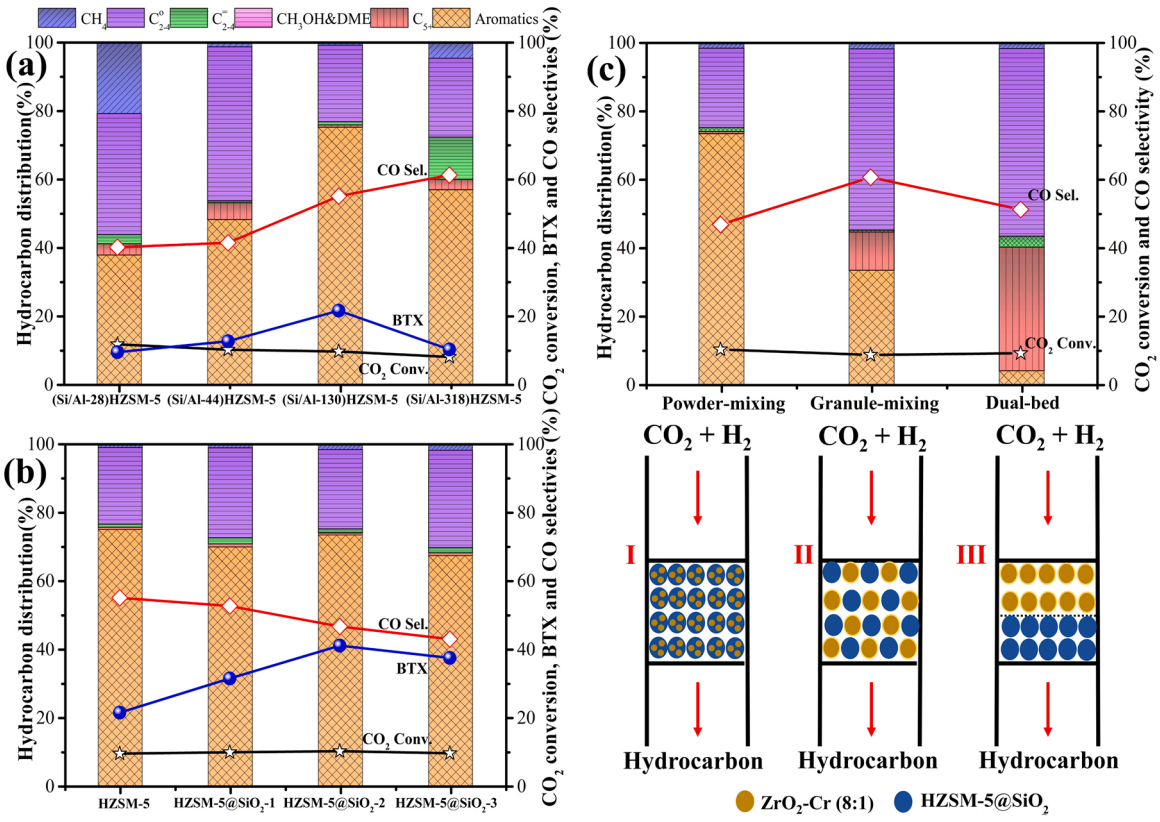

Fig. 3. Performances of CO_2 hydrogenation to light aromatics. (a) CO_2 conversion, CO selectivity and hydrocarbons distribution of sc-ZrO_2-Cr (8:1) and zeolites with different Si/Al ratios. (b) CO_2 conversion, CO selectivity and hydrocarbons distribution of sc-ZrO_2-Cr (8:1) and HZSM-5@SiO_2-X zeolites. (c) The catalytic performances of the different integration manners of aerogel catalyst and zeolites. I: Powder-mixing in an agate mortar; II: Granule-mixing; III: Dual bed. Reaction conditions: T = 360 °C, P = 4 MPa, (24.02 vol% CO_2, 4.03 vol% Ar and H_2 balance), GHSV = 1200 mL/g_{cat}/h. Catalyst weight, 0.5 g, oxide/zeolite weight ratio = 1:2.

of conducts, which was measured with XRF (Table S3).

As shown in Fig. 3(b), with increasing the amounts of SiO_2 on the external surface, the CO_2 conversion did not change much, while the CO selectivity was significantly decreased. After HZSM-5 zeolite was coated with SiO_2 layer, aromatics selectivity decreased slightly, while the selectivity of BTX was significantly improved. The BTX selectivity increased from 21.1% to 40.7% (the chromatograms of aromatics obtained from sc-ZrO_2-Cr (8:1)/HZSM-5 and sc-ZrO_2-Cr (8:1)/HZSM-5@SiO_2-2 catalysts were shown in Fig. S6 and Fig. S7). With further increasing the amounts of SiO_2 in the shell, the effective weight ratio of HZSM-5 zeolite will reduce. Moreover, this result could reduce the selectivities of total aromatics and BTX. On the other hand, excessively thick SiO_2 shell could inhibit the diffusion of methanol/dimethyl ether intermediate from oxide catalyst surface to the inside active sites of zeolite. Additionally, the driving force in the tandem process could be limited [41]. Therefore, to obtain high BTX selectivity, appropriate amounts of SiO_2 was necessary.

The porous structural evolution of the HZSM-5@SiO_2 catalyst could be also identified by N_2 adsorption-desorption isotherms (Fig. S8). The original HZSM-5 exhibited microporous properties with a sharp increase of N_2 adsorption at lower pressure. After HZSM-5 zeolite was coated with the SiO_2 shell, the specific surface area and pore volume of the core-shell structure catalyst decreased simultaneously (Table S6). These results indicated that SiO_2 was successfully deposited on the external surface of HZSM-5 zeolite. The SiO_2 shell deposition did not change the crystal structure of HZSM-5, and all zeolites exhibited the same characteristic peaks of MFI structure (Fig. S3) [42]. The acid strength and concentration of these zeolites were analyzed by NH_3-TPD [42]. Fig. S9 showed the NH_3-TPD curves of HZSM-5 and core-shell zeolites, which were coated with different amounts of SiO_2. All zeolites showed two NH_3 desorption peaks at around 175 °C and 415 °C. The introduction of SiO_2 shell resulted in a gradual shift of the desorption peak from high-temperature to the low-temperature region. Compared with the original HZSM-5 zeolite, the total acid content of HZSM-5@SiO_2 zeolite decreased with the SiO_2 shell increasing. In addition, the negative shift of the desorption peak in the high-temperature region enhanced with increasing the SiO_2 shell. In the subsequent expressions, HZSM-5@SiO_2 refers to the HZSM-5@SiO_2-2 core-shell zeolite unless otherwise specified.

To elucidate the role of tandem catalysts, the effects of the tandem catalyst with different integration manners on the catalytic performances were examined in Fig. 3(c). The tandem catalyst consisted of sc-ZrO_2-Cr (8:1) and HZSM-5@SiO_2. When sc-ZrO_2-Cr (8:1) and HZSM-5@SiO_2 were mixed by granule-mixing, the aromatics selectivity was only 33.4%. Compared with powder-mixing (Fig. 3(c, I)), the amount of C_2-C_4 alkanes increased significantly when the integration manner was granule-mixing (Fig. 3(c, II)). When the sc-ZrO_2-Cr (8:1) and HZSM-5@SiO_2 zeolites were distributed by dual bed (Fig. 3(c, III)), the aromatics selectivity further decreased to only 4% and the C_{5+} alkanes began to increase. This result indicated that the integration manners of sc-ZrO_2-Cr (8:1) and HZSM-5@SiO_2 could significantly affect the aromatics selectivity. The formation of aromatics relies on the synergistic effict of the sc-ZrO_2-Cr (8:1) oxide catalyst and HZSM-5@SiO_2 zeolite catalyst. The close spatial distance of sc-ZrO_2-Cr (8:1) and HZSM-5@SiO_2 facilitated the transfer of intermediates from the surface of sc-ZrO_2-Cr (8:1) to the HZSM-5@SiO_2, thereby enhancing the aromatics selectivity. As the spatial distance between sc-ZrO_2-Cr (8:1) and HZSM-5@SiO_2 increasing (Fig. 3(c, II and III)), the transfer of the intermediate became difficult [12]. Generally, methanol was desorbed from the sc-ZrO_2-Cr (8:1) surface and subsequently diffused into the acid sites of zeolite and further dehydrated, and cyclized to produce aromatics [43]. Light olefins were intermediates from methanol to aromatics. Increasing

the distance between aerogel catalyst and zeolite was benefical for the hydrogenation of olefins to alkanes and hindered the aromatization process [12,20,41]. These results suggested that long diffusion pathway could promote the conversion of methanol to alkanes and inhibit the production of aromatics.

3.3. Effects of aerogel catalyst composition and reaction conditions on catalytic performances

This aerogel catalyst not only maintained a high surface area, but also provided a large amount of oxygen vacancies. The formation rate of methanol intermediates on sc-ZrO_2-Cr was dominated by the total amount of oxygen vacancies. Fig. 4(a, b) showed the catalytic performances of CO_2 hydrogenation of various catalysts, which were with different Cr contents and different preparation methods at 360 °C and 4 MPa. In this part, all tandem catalysts were prepared by powder-mixing. Firstly, sc-ZrO_2 aerogel catalysts with different amounts of chromium doping were compared, as shown in Fig. 4(a). For pure sc-ZrO_2 catalyst, 3.5% CO_2 conversion and 39.3% aromatics selectivity were obtained. After sc-ZrO_2 catalyst being doped with Cr, CO_2 conversion and aromatics selectivity increased significantly. With increasing the content of doped Cr, from sc-ZrO_2-Cr (16:1) to sc-ZrO_2-Cr (1:1), aromatics selectivity displayed a volcanic pattern, which firstly increased and then decreased. After adding Cr in sc-ZrO_2 catalyst, CO_2 conversion increased slightly (Fig. 4(a)). The addition of Cr could slightly enhance the CO_2 adsorption capacity (Fig. S10). The detailed products distribution from sc-ZrO_2/HZSM-5@SiO_2-2 and sc-ZrO_2-Cr (8:1)/HZSM-5@SiO_2-2 catalysts were displayed in Table S7 and Table S8.

Fig. 4(b) compared the activities of different ZrO_2-Cr catalysts for CO_2 hydrogenation to aromatics by different prepared methods. Compared with the co-ZrO_2-Cr and the hy-ZrO_2-Cr catalysts, the sc-ZrO_2-Cr aerogel catalyst had a higher ability to activate CO_2. Aromatics selectivity increased in the following order: hy-ZrO_2-Cr<co-ZrO_2-Cr<sd-ZrO_2-Cr<sc-ZrO_2-Cr. The total CO_2 adsorption, increasing in the following order: co-ZrO_2-Cr<sd-ZrO_2-Cr<hy-ZrO_2-Cr<sc-ZrO_2-Cr, was consistent with the trend of CO_2 conversion under the same composition (Fig. S11). In addition, the adsorption of H_2 and CO on the oxide surface could be influenced by employing CO_2 supercritical drying technology. Compared with sd-ZrO_2-Cr, the sc-ZrO_2-Cr exhibited stronger adsorption capacity for H_2 (Fig. S12) and CO (Fig. S13).

On the other hand, another task of CO_2 hydrogenation was to suppress CO formation, which was from the RWGS reaction [8,21,41]. It was worth mentioning that the CO selectivity of sc-ZrO_2-Cr catalyst was also relatively low and the CH_4 selectivity was only 1.7%. In general, sc-ZrO_2-Cr (8:1)/HZSM-5@SiO_2 exhibited the best performance for BTX, which made sc-ZrO_2-Cr catalyst become an excellent candidate for direct conversion of CO_2 to BTX. To further understand the effect of reaction conditions for the production of BTX, the effects of reaction pressure and reaction temperature were compared in Fig. 4(c, d). With changing the pressure, the total aromatics selectivity in the hydrocarbons did not change significantly, while the lower pressure was beneficial to improve the BTX selectivity. BTX selectivity reached 46.8% at 3 MPa. In Fig. 4(d), increasing the reaction temperature could effectively improve CO_2

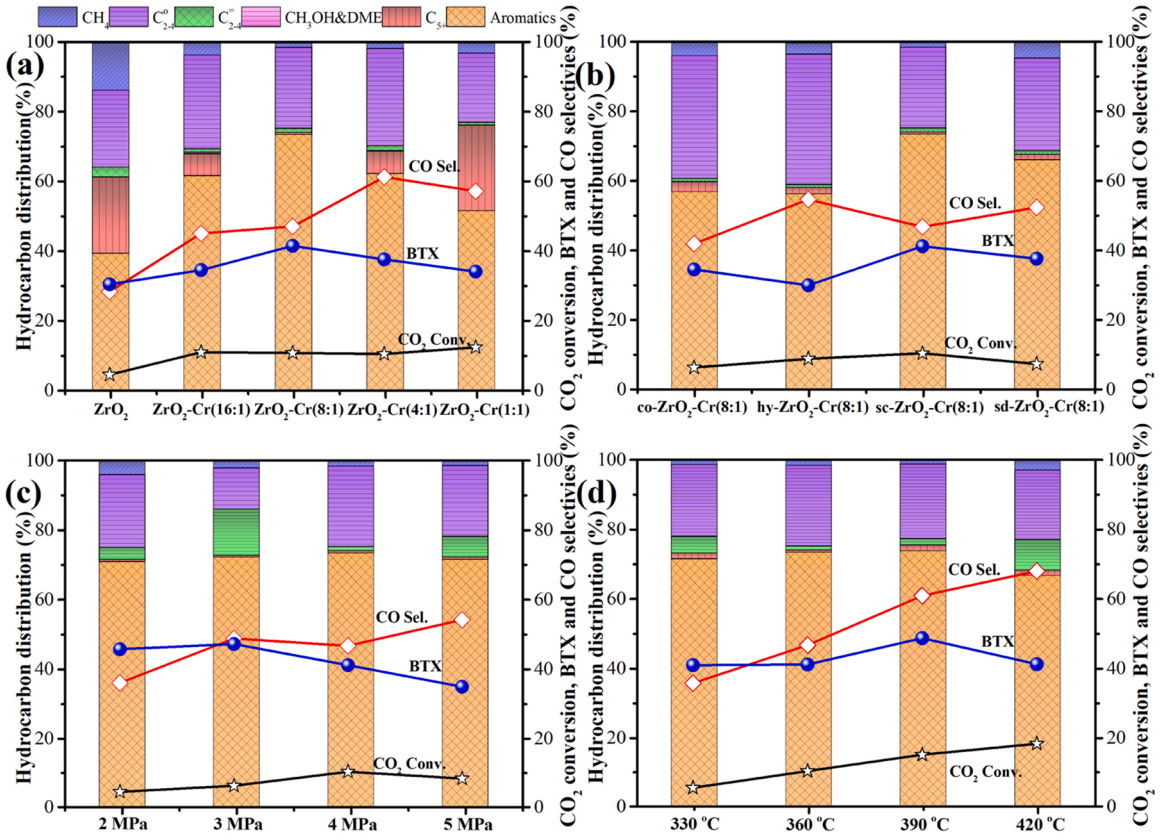

Fig. 4. Performances evaluation of Cr-doped ZrO_2 catalysts for the production of BTX. (a) Activity comparison and product distribution of Cr-doped ZrO_2 catalysts with different molar ratios of Zr/Cr. (b) CO_2 conversion and hydrocarbon distribution of ZrO_2-Cr (8:1) samples prepared by different methods. Reaction conditions: T = 360 °C, P = 4 MPa, (24.02 vol% CO_2, 4.03 vol% Ar and H_2 balance), GHSV = 1200 mL/g_{cat}/h. Catalyst weight, 0.5 g, oxide/zeolite weight ratio = 1:2. (c) CO_2 conversion and hydrocarbon distribution over the sc-ZrO_2-Cr (8:1)/HZSM-5@SiO_2 catalyst at different pressures. Reaction conditions: T = 360 °C, 24.02 vol% CO_2, 4.03 vol% Ar and H_2 balance, GHSV = 1200 mL/g_{cat}/h. Catalyst weight, 0.5 g, oxide/zeolite weight ratio = 1:2. (d) The effects of temperature on the CO_2 conversion and BTX selectivity of the sc-ZrO_2-Cr (8:1)/HZSM-5@SiO_2 catalyst. Reaction conditions: P = 4 MPa, 24.02 vol% CO_2, 4.03 vol% Ar and H_2 balance, GHSV = 1200 mL/g_{cat}/h. Catalyst weight, 0.5 g, oxide/zeolite weight ratio = 1:2.

conversion, but the CO selectivity increased simultaneously. When the reaction temperature was 390 °C, the CO_2 conversion was 14.6%, and the BTX selectivity reached 48.3%. Although increasing the reaction temperature was beneficial to improve CO_2 conversion (Fig. S14), an excessive reaction temperature could affect the generation of methanol on the sc-ZrO_2-Cr (8:1) catalyst [34]. Combining the effects of temperature and pressure, the subsequent experiments were carried out under the reaction conditions of 390 °C and 3 MPa. Over the sc-ZrO_2-Cr (8:1)/HZSM-5@SiO_2 catalyst, the CO_2 conversion, the BTX and the total aromatics selectivities reached 13.9%, 51.2%, and 76.8%, respectively, which were higher than those of other reported oxide/zeolite tandem catalyst under the same reaction conditions (Table S9).

3.4. Reaction mechanism and stability test

To further understand the reaction mechanism of CO_2 conversion over the sc-ZrO_2-Cr (8:1)/HZSM-5@SiO_2 catalyst, in-situ diffuse reflectance infrared Fourier transform spectroscopy (DRIFTS) measurements was performed, as shown in Fig. 5(a, b). For the sc-ZrO_2-Cr (8:1) metal oxide catalyst, as shown in Fig. 5(a), the peaks at 2874 and 1358 cm^{-1} were assigned to HCOO* species. The peaks at 1623, 1508 and 1341 cm^{-1} were assigned to CO_3^{2-}/bicarbonate species [2,8,41]. The peak at 3012 cm^{-1} was belonged to the C-H bond. The formation of methoxy species at around 1031 cm^{-1} was also observed. Generally, methoxy was considered to be a close intermediate for methanol [2,20,44]. For sc-ZrO_2-Cr (8:1)/HZSM-5@SiO_2 tandem catalyst, the peaks at 2874, 1623, 1358 and 1341 cm^{-1} were attributed to CO_3^{2-}/bicarbonate and the signal of HCOO* species remained (Fig. 5(b)). At the same time, a weak C-O-C stretching peak appeared at 1188 cm^{-1} for the tandem catalyst, indicating the formation of ether [8,42] on HZSM-5@SiO_2 zeolite. It was obvious that the stretching vibration at around 1685 cm^{-1} was belonged to C=C double bond [43]. In addition, the methoxyl signal at 1034 cm^{-1} decreased with increasing the reaction time [44]. Employing HZSM-5@SiO_2 core-shell zeolite resulted in a series of absorption peaks at around 1500 and 1685 cm^{-1}, due to the signals of the carbon-carbon double bond in the aromatic ring conjugated system [19,45]. The above DRIFTS results confirmed that the route of CO_2 hydrogenation to aromatics was a methanol-mediated pathway over sc-ZrO_2-Cr (8:1)/HZSM-5@SiO_2 tandem catalyst. Methanol was firstly obtained from sc-ZrO_2-Cr as an intermediate, and aromatics were formed on HZSM-5@SiO_2 zeolite. Therefore, the interaction between oxide and zeolite played a key role in this reaction, which directly controlled the production of intermediates and the final generation of aromatics [46,47]. Fig. 5(c) showed the stability evaluation of sc-ZrO_2-Cr/HZSM-5@SiO_2 at 390 °C and 3 MPa. In Fig. 5(c), the CO_2 conversion maintained stable over 40 h. CO selectivity has been decreasing for the first 15 h and then kept stable at around 29%. In addition, the aromatics selectivity decreased slightly, $C_{2-4}^{=}$ selectivity increased slightly, and the other components hardly changed during the running time. After 40 h, the aromatics selectivity leveled off around 71.6%, and BTX selectivity was 45.7%. The thermogravimetric curve of the sample after the reaction is shown in Fig. S15. There is little carbon in the zeolite, and the carbon deposit accounts for about 5.2 wt% of the sample mass.

4. Conclusions

In summary, this work has achieved high selective hydrogenation of CO_2 to light aromatics (BTX) over ZrO_2-Cr/HZSM-5@SiO_2. The one-pass CO_2 conversion was 13.9%. The light aromatics selectivity was as high

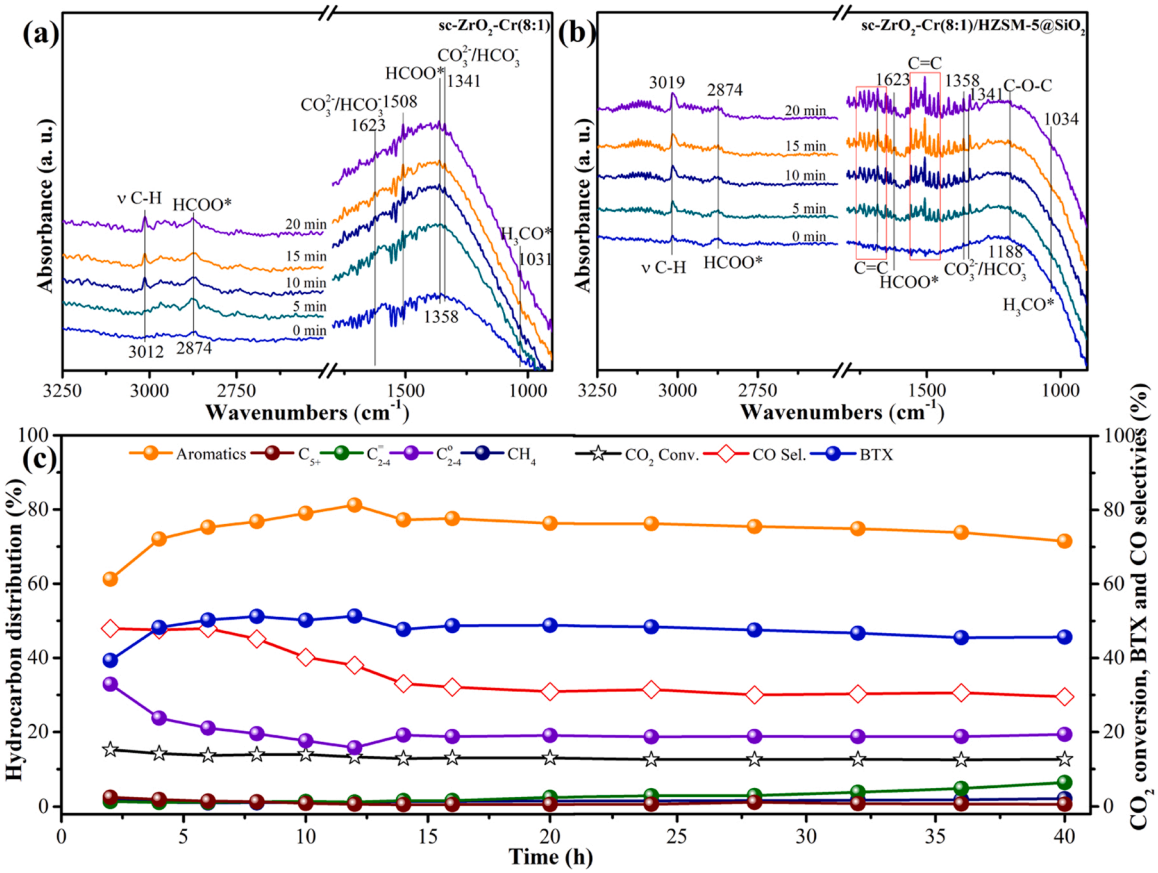

Fig. 5. In situ DRIFT spectra of CO_2 hydrogenation over (a) sc-ZrO_2-Cr (8:1) and (b) sc-ZrO_2-Cr (8:1)/HZSM-5@SiO_2 catalysts. Stability test of sc-ZrO_2-Cr/HZSM-5@SiO_2. (c) Stability test of sc-ZrO_2-Cr/HZSM-5@SiO_2. Reaction conditions: T = 390 °C, P = 3 MPa, (24.02 vol% CO_2, 4.03 vol% Ar and H_2 balance), GHSV = 1200 mL/g_{cat}/h. Catalyst weight, 0.5 g, oxide/zeolite weight ratio = 1:2.

as 51.2%, while CH_4 selectivity was only 1.1%. A highly active ZrO_2-Cr aerogels catalyst with oxygen-rich vacancies was successfully prepared by doping. Methanol was firstly generated on the surface of ZrO_2-Cr and then transformed to aromatics over the HZSM-5@SiO_2 core-shell zeolite. The synergy between ZrO_2-Cr and HZSM-5@SiO_2 effectively promoted the thermodynamic coupling CO_2 hydrogenation and the formation of aromatics. The external Brønsted acid sites of HZSM-5 zeolite were passivated through the silylation process, which could effectively inhibit the alkylation reaction of light aromatics and obtain BTX with high selectivity. The research of novel chromium-doped ZrO_2 aerogel and HZSM-5@SiO_2 core-shell zeolite tandem catalyst has opened a new avenue for highly selective conversion of CO_2 to light aromatics.

CRediT authorship contribution statement

Lijun Zhang: Investigation, Data curation, Formal analysis, Writing – original draft. **Weizhe Gao**: Conceptualization, Data curation, Methodology, Project administration, Writing – review & editing. **Fan Wang**: Data curation, Validation. **Chengwei Wang**: Data curation, Formal analysis. **Jiaming Liang**: Data curation, Validation. **Xiaoyu Guo**: Investigation, Validation. **Yingluo He**: Data curation, Investigation. **Guohui Yang**: Software, Validation. **Noritatsu Tsubaki**: Conceptualization, Data curation, Methodology, Resources, Project administration, Supervision, Writing – review & editing.

Declaration of Competing Interest

The authors declare that they have no known competing financial interests or personal relationships that could have appeared to influence the work reported in this paper.

Data Availability

No data was used for the research described in the article.

Acknowledgments

Financial support from MIRAI project of Japan Science and Technology Agency (JST) is greatly appreciated (JPMJMI17E2). NEDO of Japan provided research funds. F. Wang acknowledges financial support from the Regional Industrial Innovation and Creation Fellowship in University of Toyama.

Appendix A. Supporting information

Supplementary data associated with this article can be found in the online version at doi:10.1016/j.apcatb.2023.122535.

References

[1] Jie Li, Yingluo He, Li Tan, Peipei Zhang, Xiaobo Peng, Anjaneyulu Oruganti, Guohui Yang, Hideki Abe, Ye Wang, Noritatsu Tsubaki, Integrated tuneable synthesis of liquid fuels via Fischer-Tropsch technology, Nat. Catal. 1 (2018) 787–793.
[2] Yang Wang, Li Tan, Minghui Tan, Peipei Zhang, Yuan Fang, Yoshiharu Yoneyama, Guohui Yang, Noritatsu Tsubaki, Rationally designing bifunctional catalysts as an efficient strategy to boost CO_2 hydrogenation producing value-added aromatics, ACS Catal. 9 (2019) 895–901.
[3] Yanfei Xu, Jingge Liu, Jie Wang, Guangyuan Ma, Jianghui Lin, Yong Yang, Yongwang Li, Chenghua Zhang, Mingyue Ding, Selective conversion of syngas to aromatics over Fe_3O_4@MnO_2 and hollow HZSM-5 bifunctional catalysts, ACS Catal. 9 (2019) 5147–5156.
[4] Haiyan Yang, Chen Zhang, Peng Gao, Hui Wang, Xiaopeng Li, Liangshu Zhong, Wei Wei, Yuhan Sun, A review of catalytic hydrogenation of carbon dioxide into value-added hydrocarbons, Catal. Sci. Technol. 7 (2017) 4580–4598.
[5] Peng Gao, Shenggang Li, Xianni Bu, Shanshan Dang, Ziyu Liu, Hui Wang, Liangshu Zhong, Minghuang Qiu, Chengguang Yang, Jun Cai, Wei Wei, Yuhan Sun, Direct conversion of CO_2 into liquid fuels with high selectivity over a bifunctional catalyst, Nat. Chem. 9 (2017) 1019–1024.
[6] Alexander M. Niziolek, Onur Onel, Christodoulos A. Floudas, Production of benzene, toluene, and xylenes from natural gas via methanol: process synthesis and global optimization, Comput. Aided Chem. Eng. 62 (2016) 1531–1556.
[7] Christian Baltes, Sascha Vukojević, Ferdi Ferdinand Schüth, Correlations betweensynthesis, precursor, and catalyst structure and activity of a large set of CuO/ZnO/Al_2O_3 catalysts for methanol synthesis, J. Catal. 258 (2008) 334–344.
[8] Cheng Zhou, Jiaqing Shi, Wei Zhou, Kang Cheng, Qinghong Zhang, Jincan Kang, Ye Wang, Highly Active ZnO-ZrO_2 Aerogels Integrated with H-ZSM-5 for Aromatics Synthesis from Carbon Dioxide, ACS Catal. 10 (2020) 302–310.
[9] Malte Behrens, Felix Studt, Igor Kasatkin, Stefanie Kühl, Michael Hävecker, Frank Abild-Pedersen, Stefan Zander, Frank Girgsdies, Patrick Kurr, Benjamin-Louis Kniep, Michael Tovar, Richard W. Fischer, Jens K. Nørskov, Robert Schlögl, The active site of methanol synthesis over Cu/ZnO/Al_2O_3 industrial catalysts, Science 336 (2012) 893–897.
[10] Roy van den Berg, Gonzalo Prieto, Gerda Korpershoek, Lars I. van der Wal, Arnoldus J. van Bunningen, Susanne Lægsgaard-Jørgensen, Petra E. de Jongh, Krijn P. de Jong, Structure sensitivity of Cu and CuZn catalysts relevant to industrial methanol synthesis, Nat. Commun. 7 (2016) 13057.
[11] Unni Olsbye, Stian Svelle, Morten Bjørgen, Pablo Beato, Ton V.W. Janssens, Finn Joensen, Silvia Bordiga, Karl Petter Lillerud, Conversion of methanol to hydrocarbons: how zeolite cavity and pore size controls product selectivity, Angew. Chem. Int. Ed. 51 (2012) 5810–5831.
[12] Zelong Li, Yuanzhi Qu, Jijie Wang, Hailong Liu, Mingrun Li, Shu Miao, Can Li, Highly selective conversion of carbon dioxide to aromatics over tandem catalysts, Joule 3 (2019) 570–583.
[13] Peng Gao, Shanshan Dang, Shenggang Li, Xianni Bu, Ziyu Liu, Minghuang Qiu, Chengguang Yang, Hui Wang, Liangshu Zhong, Yong Han, Qiang Liu, Wei Wei, Yuhan Sun, Direct production of lower olefins from CO_2 conversion via bifunctional catalysis, ACS Catal. 8 (2018) 571–578.
[14] Yi Fu, Youming Ni, Wenhao Cui, Xudong Fang, Zhiyang Chen, Zhaopeng Liu, Wenliang Zhu, Zhongmin Liu, Insights into the size effect of ZnCr2O4 spinel oxide in composite catalysts for conversion of syngas to aromatics, Green Energy & Environment, doi.org/10.1016/j.gee.2021.07.003.
[15] Jian Wei, Qingjie Ge, Ruwei Yao, Zhiyong Wen, Chuanyan Fang, Lisheng Guo, Hengyong Xu, Jian Sun, Directly converting CO_2 into a gasoline fuel, Nat. Commun. 8 (2017) 15174.
[16] Shyam Kattel, Ping Liu, Jingguang G. Chen, Tuning selectivity of CO_2 hydrogenation reactions at the metal/oxide interface, J. Am. Chem. Soc. 139 (2017) 9739–9754.
[17] Adrian Ramirez, Abhay Dokania, Pieter Cnudde, Mustafa Caglayan, Irina Yarulina, Edy Abou-Hamad, Lieven Gevers, Samy Ould-Chikh, Kristof De Wispelaere, Veronique van Speybroeck, Jorge Gascon, Effect of zeolite topology and reactor configuration on the direct conversion of CO_2 to light olefins and aromatics, ACS Catal. 9 (2019) 6320–6334.
[18] Xu Cui, Peng Gao, Shenggang Li, Chengguang Yang, Ziyu Liu, Hui Wang, Liangshu Zhong, Yuhan Sun, Selective production of aromatics directly from carbon dioxide hydrogenation, ACS Catal. 9 (2019) 3866–3876.
[19] Kang Cheng, Wei Zhou, Jincan Kang, Shun He, Shulin Shi, Qinghong Zhang, Yang Pan, Wu Wen, Ye Wang, Bifunctional catalysts for one-step conversion of syngas into aromatics with excellent selectivity and stability, Chem 3 (2017) 334–347.
[20] Weizhe Gao, Lisheng Guo, Qinming Wu, Chengwei Wang, Xiaoyu Guo, Yingluo He, Peipei Zhang, Guohui Yang, Guangbo Liu, Jinhu Wu, Noritatsu Tsubaki, Capsule-like zeolite catalyst fabricated by solvent-free strategy for para-Xylene formation from CO_2 hydrogenation, Appl. Catal. B: Environ. 303 (2022), 120906.
[21] Jian Wei, Ruwei Yao, Qingjie Ge, Dongyan Xu, Chuanyan Fang, Jixin Zhang, Hengyong Xu, Jian Sun, Precisely regulating Brønsted acid sites to promote the synthesis of light aromatics via CO_2 hydrogenation, Appl. Catal. B: Environ. 283 (2021), 119648.
[22] Xinbao Zhang, Anfeng Zhang, Xiao Jiang, Jie Zhu, Junhui Liu, Junjie Li, Guanghui Zhang, Chunshan Song, Xinwen Guo, Utilization of CO_2 for aromatics production over ZnO/ZrO_2-ZSM-5 tandem catalyst, J. CO_2 Util. 29 (2019) 140–145.
[23] Youming Ni, Zhiyang Chen, Yi Fu, Yong Liu, Wenliang Zhu, Zhongmin Liu, Selective conversion of CO_2 and H_2 into aromatics, Nat. Commun. 9 (2018) 3457.
[24] Junfeng Zhang, Meng Zhang, Shuyao Chen, Xiaoxing Wang, Zeling Zhou, Yingquan Wu, Tao Zhang, Guohui Yang, Yizhuo Han, Yisheng Tan, Hydrogenation of CO_2 into aromatics over a ZnCrOx-zeolite composite catalyst, Chem. Commun. 55 (2019) 973–976.
[25] Muhammad Tahir Arslan, Babar Ali, Syed Zulfiqar Ali Gilani, Yilin Hou, Qi Wang, Dali Cai, Yao Wang, Fei Wei, Selective conversion of syngas into tetramethylbenzene via an aldol-aromatic mechanism, ACS Catal. 10 (4) (2020) 2477–2488.
[26] Haiqun Xu, Sizhuo Yang, Xing Ma, Jier Huang, Hailong Jiang, Unveiling charge-separation dynamics in CdS/Metal-Organic framework composites for enhanced photocatalysis, ACS Catal. 8 (2018) 11615–11621.
[27] Mittal Jagjiwan, Konno Hidetaka, Inagaki Michio I, Synthesis of graphite intercalation compounds with Cr^{VI} compounds using CrO_3 and HCl at room temperature, Synth. Met. 96 (1998) 103–108.
[28] Heng Zhao, Lisheng Guo, Weizhe Gao, Fei Chen, Xuemei Wu, Kangzhou Wang, Yingluo He, Peipei Zhang, Guohui Yang, Noritatsu Tsubaki, Multi-Promoters regulated iron catalyst with well-matching reverse water-gas shift and chain propagation for boosting CO_2 hydrogenation, J. CO_2 Util. 52 (2021), 101700.
[29] Yifeng Zhu, Xiulian Pan, Feng Jiao, Jian Li, Junhao Yang, Minzheng Ding, Yong Han, Zhi Liu, Xinhe Bao, Role of manganese oxide in syngas conversion to light olefins, ACS Catal. 7 (2017) 2800–2804.

[30] Fengcai Lei, Yongfu Sun, Katong Liu, Shan Gao, Liang Liang, Bicai Pan, Yi Xie, Oxygen vacancies confined in ultrathin indium oxide porous sheets for promoted visible-light water splitting, J. Am. Chem. Soc. 136 (2014) 6826–6829.
[31] Weizhe Gao, Lisheng Guo, Yu Cui, Guohui Yang, Yingluo He, Chunyang Zeng, Akira Taguchi, Takayuki Abe, Qingxiang Ma, Yoshiharu Yoneyama, Noritatsu Tsubaki, Selective conversion of CO_2 into para-Xylene over a $ZnCr_2O_4$-ZSM-5 Catalyst, ChemSusChem 13 (2020) 6541–6545.
[32] Michael Schneider, Alfons Baiker, Aerogels in catalysis, Catal. Rev. 37 (1995) 515–556.
[33] Pajonk, G.érard Marcel, Catalytic aerogels, Catal. Today 35 (1997) 319–337.
[34] Jijie Wang, Guanna Li, Zelong Li, Chizhou Tang, Zhaochi Feng, Hongyu An, Hailong Liu, Taifeng Liu, Can Li, A highly selective and stable ZnO-ZrO_2 solid solution catalyst for CO_2 hydrogenation to methanol, Sci. Adv. 3 (2017), e1701290.
[35] Qingxiang Ma, Lisheng Guo, Yuan Fang, Hangjie Li, Jiangli Zhang, Tiansheng Zhao, Guohui Yang, Yoshiharu Yoneyama, Noritatsu Tsubaki, Combined methane dry reforming and methane partial oxidization for syngas production over high dispersion Ni based mesoporous catalyst, Fuel Process. Technol. 188 (2019) 98–104.
[36] Huiqing Song, Daniel Laudenschleger, John J. Carey, Holger Ruland, Michael Nolan, Martin Muhler, Spinel structured $ZnCr_2O_4$ with excess Zn is the active ZnO/Cr_2O_3 catalyst for high temperature methanol synthesis, ACS Catal. 7 (2017) 7610–7622.
[37] Jian Zhang, Liang Wang, Zhiyi Wu, Hai Wang, Chengtao Wang, Shichao Han, Feng-Shou Xiao, Solvent-Free synthesis of core-shell Zn/ZSM-5@Silicalite-1 catalyst for selective conversion of methanol to BTX aromatics, Ind. Eng. Chem. Res. 58 (34) (2019) 15453–15458.
[38] Shourong Zheng, Hilton R. Heydenrych, Andreas Jentys, Johannes A. Lercher, Influence of surface modification on the acid site distribution of HZSM-5, J. Phys. Chem. B 106 (2002) 9552–9558.
[39] Jingui Zhang, Weizhong Qian, Chuiyan Kong, Fei Wei, Increasing para-Xylene selectivity in making aromatics from methanol with a Surface-Modified Zn/P/ZSM-5 catalyst, ACS Catal. 5 (2015) 2982–2988.
[40] Yajing Wang, Weiteng Zhan, Zhijie Chen, Jianmin Chen, Xingang Li, Yingwei Li, Advanced 3D Hollow-Out ZnZrO@C combined with hierarchical zeolite for highly active and selective CO hydrogenation to aromatics, ACS Catal. 10 (2020) 7177–7187.
[41] Yang Wang, Weizhe Gao, Shun Kazumi, Hangjie Li, Guohui Yang, Noritatsu Tsubaki, Direct and oriented conversion of CO_2 to Value-Added aromatics, Chem. -A Eur. J. 25 (2019) 5149–5153.
[42] Zilacleide S.B. Sousa, Cláudia O. Veloso, Cristiane A. Henrique, Victor Teixeira da Silv, Ethanol conversion into olefins and aromatics over HZSM-5 zeolite: influence of reaction conditions and surface reaction studies, J. Mol. Catal. A 422 (2016) 266–274.
[43] Yang Wang, Weizhe Gao, Kangzhou Wang, Xinhua Gao, Baizhang Zhang, Heng Zhao, Qingxiang Ma, Peipei Zhang, Guohui Yang, Mingbo Wu, Noritatsu Tsubaki, Boosting the synthesis of value-added aromatics directly from syngas via a Cr_2O_3 and Ga doped zeolite capsule catalyst, Chem. Sci. 12 (2021) 7786–7792.
[44] Xin Shang, Guodong Liu, Xiong Su, Yanqiang Huang, Tao Zhang, Preferential synthesis of toluene and xylene from CO_2 hydrogenation in the presence of benzene through an enhanced coupling reaction, ACS Catal. 12 (2022) 13741–13754.
[45] Nicola Hüsing, Ulrich Schubert, Aerogels-Airy materials: chemistry, structure, and properties, Angew. Chem. Int. Ed. 37 (1998) 22–45.
[46] Kongzhai Li, Jingguang G. Chen, CO_2 hydrogenation to methanol over ZrO_2-containing catalysts: Insights into ZrO_2 induced synergy, ACS Catal. 9 (2019) 7840–7861.
[47] Erwin Lam, Kim Larmier, Shohei Tada, Patrick Wolf, Olga V. Safonova, Christophe Copéret, Zr(IV) surface sites determine CH_3OH formation rate on Cu/ZrO_2/SiO_2-CO_2 hydrogenation catalysts, Chin. J. Catal. 40 (2019) 1741–1748.